Commissioning of a compact laser-based proton beam line for high intensity bunches around 10 MeV

S. Busold,[1,*] D. Schumacher,[2,†] O. Deppert,[1] C. Brabetz,[3] F. Kroll,[4,5] A. Blažević,[2,6] V. Bagnoud,[2,6] and M. Roth[1]

[1]*Institut für Kernphysik, Technische Universität Darmstadt, Schloßgartenstraße 9, D-64289 Darmstadt, Germany*

[2]*GSI Helmholtzzentrum für Schwerionenforschung, Planckstraße 1, D-64291 Darmstadt, Germany*

[3]*Institut für angewandte Physik, Johann-Wolfgang-Goethe Universität Frankfurt, Max von Laue Straße 1, D-60438 Frankfurt, Germany*

[4]*Helmholtz-Zentrum Dresden—Rossendorf, Bautzner Landstraße 400, D-01328 Dresden, Germany*

[5]*Technische Universität Dresden, D-01062 Dresden, Germany*

[6]*Helmholtz Institut Jena, Helmholtzweg 4, D-07734 Jena, Germany*

(Received 25 November 2013; published 17 March 2014)

We report on the first results of experiments with a new laser-based proton beam line at the GSI accelerator facility in Darmstadt. It delivers high current bunches at proton energies around 9.6 MeV, containing more than 10^9 particles in less than 10 ns and with tunable energy spread down to 2.7% ($\Delta E/E_0$ at FWHM). A target normal sheath acceleration stage serves as a proton source and a pulsed solenoid provides for beam collimation and energy selection. Finally a synchronous radio frequency (rf) field is applied via a rf cavity for energy compression at a synchronous phase of −90 deg. The proton bunch is characterized at the end of the very compact beam line, only 3 m behind the laser matter interaction point, which defines the particle source.

DOI: 10.1103/PhysRevSTAB.17.031302 PACS numbers: 52.38.Kd, 52.59.-f, 41.75.Jv

I. INTRODUCTION

Laser-based ion acceleration as a source for intense, MeV-range ion bunches has been discussed for many possible applications since their discovery. They range from fusion science [1], warm dense matter creation [2–4], and diagnostic [5–7] up to medical applications [8,9].

A well-understood and widely-used mechanism for laser-based ion acceleration is the TNSA machanism (target normal sheath acceleration, [10,11]). It is most efficiently used for accelerating protons and shows excellent beam properties with respect to bunch intensity and emittance [12]. However, the beam suffers from large envelope divergence and a continuous energy spectrum, while for most applications a low divergent, monoenergetic bunch is necessary. Therefore, much effort has been taken to face these problems in the past years. Most promising results could be achieved by applying magnetic fields for chromatic focusing, thus collimate the beam and provide for a first energy selection at the same time. Pulsed solenoids [13,14] and permanent magnetic quadrupoles [15,16] have been reported as suitable options.

Still, the energy spread of the obtained bunches is high and energy compression necessary. This can be done with a synchronous radio frequency (rf) field and has been experimentally demonstrated first by Ikegami *et al.* [17] and later improved by Nishiuchi *et al.* [16]. They were able to build an integrated test beam line at 1 Hz for protons up to 2.2 MeV energy with an energy spread of 5% and medium particle numbers of about 5×10^6 protons in the final bunch. Apart from this Japanese group, interest in such a beam line arises now in other groups around the world, too [18,19].

In Germany, the LIGHT collaboration [20] has built such a test beam line at the GSI Helmholtz center for heavy ion research as a central part of the collaboration's agenda. It differs, however, significantly from the Japanese one, as it is designed for higher energies, highest bunch intensities, and a final energy spread of less than 3%. In this paper, we introduce this new beam line and present its first experimental results.

II. EXPERIMENTAL SETUP

The experiments were performed at GSI Darmstadt with the PHELIX laser [21], which is able to accelerate protons to multi-MeV energies from thin foil targets via the TNSA mechanism. A pulsed high-field solenoid is used for collimation and transport of the bunch. A detailed

*Corresponding author.
s.busold@gsi.de
†de.schumacher@gsi.de

FIG. 1. The 15 cm long pulsed solenoid is positioned 8 cm behind the laser target and is typically set to focus 9.6 MeV protons at 3 m (maximum field at the solenoid of 7.5 T). The cavity (550 mm long) starts at 2 m and is followed by a diagnostic box around 3 m, where RCF stacks, a diamond ToF detector and a magnetic dipole detector can be placed (details in text).

description of this first stage of the beam line including a full characterization of the proton bunch can be found in a previous publication [22]. Similar targets (5 and 10 μm thin flat gold foils) and laser parameters (laser pulse duration $\tau = 650$ fs, focal spot size 3.5×3.5 μm^2 (at FWHM) and 10–15 J of laser energy on target, thus laser intensities exceeding 10^{19} W/cm^2) were used.

The rf cavity has been implemented most recently and is positioned 2 m behind the laser matter interaction point, see Fig. 1. This present paper will focus on our experiments with the cavity and refers to our previous paper concerning the earlier stages of the beam line up to the cavity. The cavity is a spiral resonator with a resonance frequency of 108.4 MHz and is attached to the rf infrastructure of GSI's universal linear accelerator (UNILAC). It is 550 mm long and contains three gaps of 20 mm (1st and 3rd) and 40 mm (2nd gap) length with 150 mm drift tubes separating them. The overall applied voltage across all three gaps is in excess of 1 MV (ratio at the gaps 1 : 2 : 1) at 100 kW input rf power.

III. CHARACTERIZATION OF THE FOCUSED BEAM AT 3 METERS

The characterization of the bunch at 3 m distance to the source is performed by two independent methods. First, a diamond detector is used for time-of-flight (ToF) measurements to determine the reference energy spectrum of the proton bunch without applied rf. Its description can be found in [22]. Figure 2 shows the recorded ToF signal and the resulting proton spectrum when focusing 8.8 MeV at the detection position of 3 m behind the laser target (i.e., $B_{z,\max} = 7.3$ T). Although (solely) these measurements have been performed at a slightly different focusing field, the results can be compared to the results of focusing 9.6 MeV (i.e., $B_{z,\max} = 7.5$ T) as no significant difference in the spectral shape with respect to the central energy is to be expected.

The central region of the proton spectrum can be fitted by a Gaussian distribution function with a central energy $E_0 = 8.76$ MeV and a standard deviation of $\sigma = 0.70$ MeV.

The comparative detection method is the radiochromic imaging spectroscopy (RIS, [23]), which is an established and well-known technique in the community of laser-based proton acceleration. It makes use of radiation sensitive radiochromic films (RCFs) in a stacked configuration and

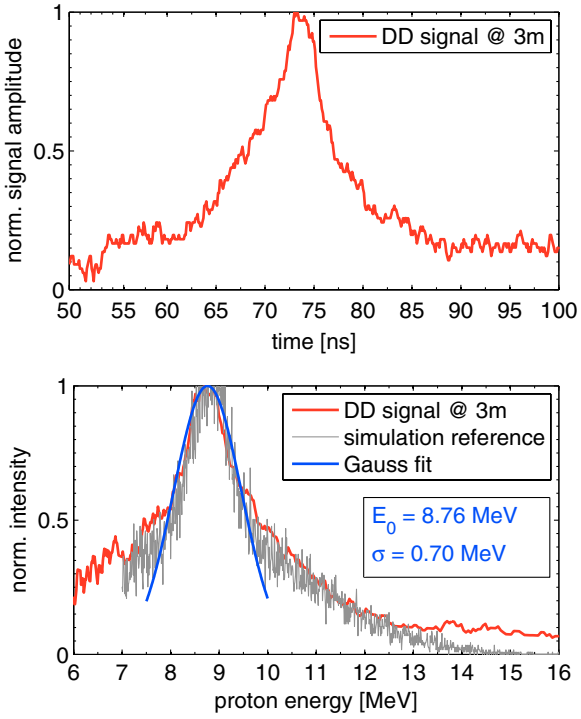

FIG. 2. ToF results from the diamond detector (upper picture) and obtained proton spectrum (lower picture) for the case of focusing 8.8 MeV protons at 3 m, for which the FWHM is 8.6 ns (ToF) or 1.6 MeV (energy spectrum). A Gaussian with a $\sigma =$ 0.70 MeV fits the central part of the bunch well. Also indicated is the particle spectrum used in the comparative simulations.

is able to fully characterize a typical TNSA proton beam. The spectral resolution of this technique is limited to the finite thickness of each RCF, which consists of a thin sensitive layer and a thicker plastic substrate. It is, however, possible to improve the spectral resolution at the expanse of spatial resolution: placing for example a thin metal foil, which only covers half of the transverse beam profile, in front of the RCF, results in two different Bragg energies in the RCF's active layer due to the additional thickness of the foil that the protons of the one half-space have to pass compared to the protons of the other half-space. The term *Bragg energy* here defines the proton energy with the highest energy loss in the active layer, which is the proton that is stopped at the end of the active layer (due to the characteristic energy deposition of an ion in matter, which is described by the Bragg curve). The difference ΔE between both Bragg energies is adjusted by the thickness of this foil. Partitioning the transverse beam profile now further and using different foil thicknesses for each section results in as many different Bragg energies mapped in the active layer as different thicknesses are used. Also, of course, every RCF in a such modified stack of RCFs gets the imprint of different Bragg energies in its active layer. In our case, a specially designed copper spacer is used in front of the RCF stack, that allowed us to map 11 different Bragg

energies throughout three RCFs in a small area of $3/20 \times 3/20$ inch^2 and covers the full transverse beam profile with a regular grid of these pixels, thus enabling a resolution between the single layers of 0.5 MeV for the energy interval of (9.5 ± 2) MeV while still obtaining a transverse beam profile for each energy that covers 1/3 of the transverse profile for the central energies [(9.5 ± 1) MeV]. As the outer layers cover only 1/9 of the detection area, the deposited energy is downscaled by a factor of 3 for the central layers in the analysis method to ensure the correct relative values. This has to be taken into account when finally calculating absolute particle numbers.

The RCF results shown in this paper are all obtained using this technique in combination with type EBT3 RCFs. The main advantages of this method are that the full transverse beam profile is detected and that the films are absolutely calibrated, thus proton numbers can be calculated.

As already shown with the ToF detector, the proton spectrum can be assumed to be of a Gaussian shape around a central energy E_0, which is the relevant area for the energy compression. Particles with higher or lower energies cannot be captured within one rf bucket (i.e., a single bunch), but will be longitudinally deflected to a satellite energy. Therefore, only the central part of the bunch will be considered further on in the analysis. Consequently, for the RCF technique, a Gaussian-like distribution function is assumed:

$$\frac{dN}{dE} = \frac{N_0}{E} \times \exp\left[-\frac{(E - E_0)^2}{2\sigma^2}\right] \quad (1)$$

with the free fit parameters σ (the standard deviation, giving access to the energy spread) and N_0 (to obtain absolute particle numbers). The parameter E_0 is determined by the field strength of the solenoid and will in general be influenced by the rf field of the cavity depending on the synchronous phase. Therefore it will be treated separately in the experiments with rf.

The solenoid is set to focus the energy of interest at 3 m behind the laser target and therefore behind the cavity. Focusing 9.6 MeV protons (i.e., a maximum longitudinal magnetic field within the solenoid of $B_{z,\max} = 7.5$ T; this is the used standard configuration for the presented experiments) results in a deposited energy profile in the RCFs as shown in Fig. 3 and fits well with the expected deposited energy profile of a Gaussian distribution [see Eq. (1)] with $E_0 = (9.6 \pm 0.1)$ MeV and $\sigma = (0.72 \pm 0.06)$ MeV. The error is dominated by the uncertainty of E_0 due to uncertainties of the Bragg energies for each layer (± 0.1 MeV). Furthermore, particle numbers and transverse beam profile can be obtained with the RCF method. In the experiments at hand, the proton numbers in the central region are in excess of 10^9 and the transverse beam dimensions are 15×15 mm^2. This is because of the very smooth focusing of the solenoid, its field aberrations, and the beam profile modulation caused by comoving electrons

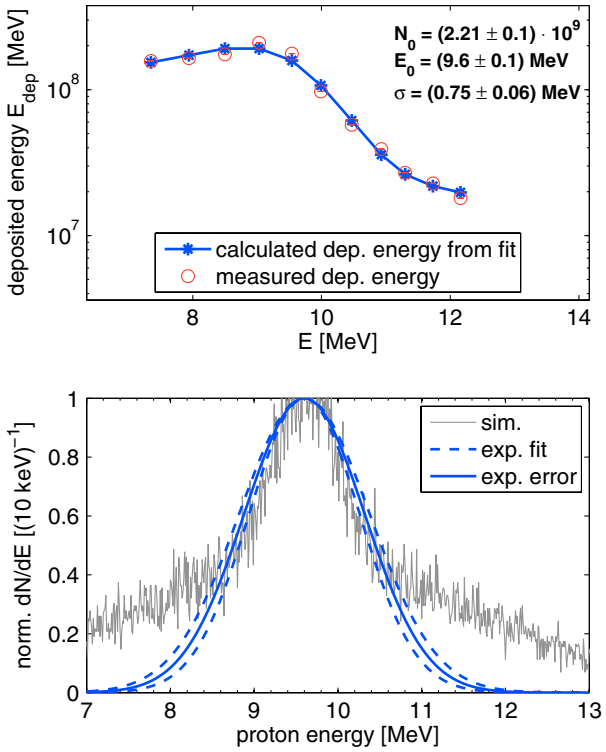

FIG. 3. Deposited energy in the RCFs when focusing 9.6 MeV at 3 m to the laser target. A Gaussian spectral distribution with an energy width of $\sigma = (0.72 \pm 0.06)$ MeV [compare Eq. (1)] can be deduced by deconvolution. The calculated deposited energy from such a Gaussian distribution fits the measured deposited energy very well.

within the solenoid (compare [22]) as well as the fact that the bunch has a large energy spread and the focal spot size at one detection position is different for every energy. A reduction in beam size could be achieved by adding an additional focusing element (e.g., second solenoid or quadrupole doublet) to the beam line.

Also shown in Fig. 3 (lower graph) is the obtained Gaussian particle distribution, which fits very well the relevant central part of the spectrum (for reference here the particle spectrum from the comparative simulations is shown, which has been adapted to the measured spectral shape via the ToF detector).

Finally, a magnetic dipole spectrometer is used for the calibration of the injection phase. The bunch passes a 6×2 mm^2 aperture and propagates through three identical permanent magnetic dipoles, each 6 cm long and with a central field of 1.2 T. The dispersed bunch is then detected with RCFs again and information about central bunch energy (position of the recorded proton trace) and energy spread (length of the recorded proton trace) can be obtained. A measurement of the magnetic field distribution and a simulation of the spectrometer with the commercial program *CST particle studio* [24] to obtain the dispersion relation was performed prior to the experiments.

Comparative simulation studies have been done to describe the effect of the rf to the proton bunch, too. The simulations shown in this paper were obtained with the code TRACEWIN [25]. The simulated bunch's input energy spectrum is modeled according to the measured, realistic spectral shape as indicated in Fig. 2. This is accomplished by a superposition of two Gaussian distributions: One with a $\sigma = 0.70$ MeV to model the (relevant) central part and another with a $\sigma = 2.1$ MeV to take into account for the edge behavior (compare *simulation reference* in Fig. 2).

IV. SYNCHRONIZING LASER AND RF

The PHELIX laser is synchronized precisely (remaining jitter of 0.3 ns) to the rf, thus the synchronous phase Φ_s is adjustable in advance with a precision of $\Delta\Phi_s = \pm 12$ deg. An exact relative measurement of the timing between the laser incidence and the rf phase is done on-shot by detecting the passing laser pulse with a photodiode behind one of the last (leaky) mirrors before entering the target chamber and measuring the phase within the cavity in parallel (precision: $\Delta\Phi_s = \pm 2$ deg). For absolute values, calibration via a complementary absolute measurement method is necessary and performed with the dipole spectrometer. The trace length of the detected dispersed bunch is a measure of the energy spread. Varying the injection phase by varying the relative delay between laser and rf results in an observed minimum trace length at the dipole spectrometer (see Fig. 4 upper graph), defining $\Phi_s = -90$ deg at a relative delay between laser and rf of 3.4 ns. This was done for two different gap voltages, which are normalized to the observed optimum value in retrospective.

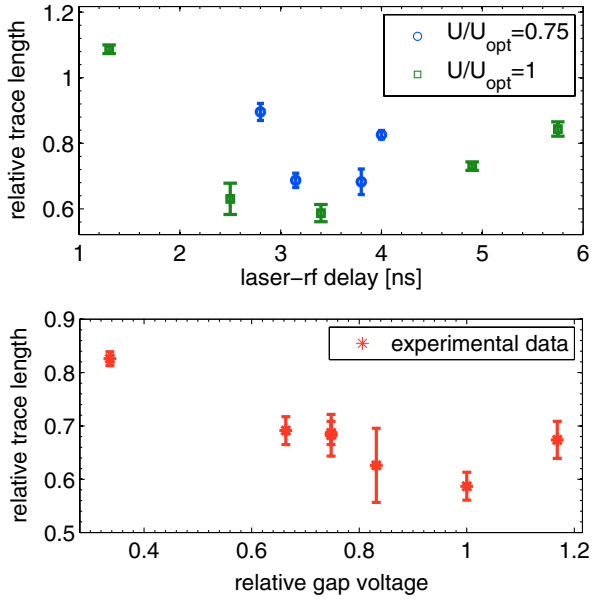

FIG. 4. The trace length on the dipole spectrometer is a measure of the energy spread. The minimum occurs at an injection phase of −90 deg (upper graph). At this injection phase, the rf power is varied to find the optimum working point (again the minimum, lower graph).

Afterward, the rf power is varied at this injection phase to finally determine the optimum working parameters for energy compression (see Fig. 4 lower graph). It is observed that the energy spread increases again at higher rf power. This indicates an *overrotated* bunch in longitudinal phase space and allows for phase focusing along a drift. All applied gap voltages U are shown relative to this optimum voltage U_{opt}, as an absolute measurement of the gap voltage is not possible. An estimate can be given with regard to rf input power P and the cavity's shunt impedance R_s via $U_{opt} \approx \sqrt{2PR_s} = 1$ MV.

V. RESULTS ON ENERGY COMPRESSION

The operation of the beam line is foreseen at an injection phase of −90 deg for energy compression. In this area, also a peaked proton spectrum is to be expected around a central energy E_0, which depends on the exact injection phase, which again is measured with high precision on-shot. The RCF technique is exploited to characterize the proton bunches.

At $\Phi_s = -78$ deg, the central energy is slightly shifted to $E_0 = 9.7$ MeV. With the assumption of a Gaussian-like spectrum, the corresponding particle spectrum can be obtained from the deposited energy profile in the RCF data by deconvolution and a standard deviation of $\sigma = (0.11 \pm 0.07)$ MeV is obtained, i.e., an energy spread at FWHM of $\Delta E/E_0 = 2.35\sigma/E_0 = (2.7 \pm 1.7)\%$. Measured and fitted deposited energy profile are shown in Fig. 5 (upper graph) as well as the resulting spectral profile (lower graph), including an ideally calculated spectrum from tracking simulations.

A similar analysis was done for $\Phi_s = -32$ deg and $\Phi_s = -137$ deg. Again the central energy is obtained from the measurement of the synchronous phase ($E_0 = 10.15$ MeV and $E_0 = 9.2$ MeV). The calculated energy spread at FWHM in the experiment is $(3.1 \pm 1.7)\%$ and $(5.3 \pm 2.7)\%$, respectively and therefore shows again an increasing energy spread and the correct energy shift as expected, although the simulations again predict even smaller values in the ideal case, see Fig. 6.

For the calculation of the particle numbers, one has to take into account that each energy layer covers only 1/3 of the full transverse beam profile and that the deposited energy has been downscaled by a factor of 3 for the central energies. Thus, for the particle number calculation, the distribution function is numerically integrated (between ±FWHM/2) and multiplied by a factor of 9. This reveals a proton number of 1.7×10^9 (±15%) within the FWHM for the case of $\Phi_s = -78$ deg (Fig. 5) and likewise 1.2×10^9 (±17%) for $\Phi_s = -32$ deg and 8.7×10^8 (±5%) for $\Phi_s = -137$ deg. In general, particle number fluctuations like these (and up to a factor of 3) have to be expected from

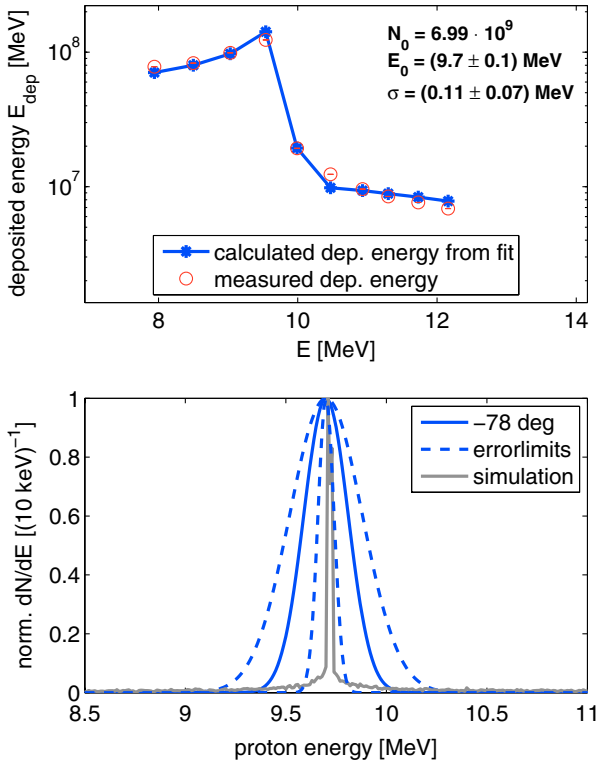

FIG. 5. Shown are the measured deposited energy profile in the RCFs and the calculated one by the fit (upper graph), and the obtained particle spectrum at $\Phi_s = -78$ deg including a simulation reference (lower graph).

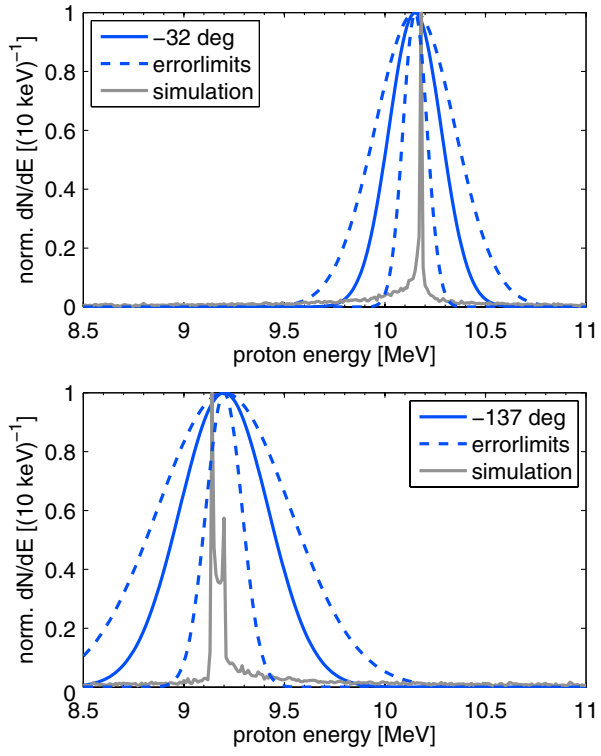

FIG. 6. The measured and simulated particle spectra for $\Phi_s = -32$ deg and $\Phi_s = -137$ deg.

the laser-driven source and were also observed in earlier experiments.

VI. TOWARD HIGHEST BUNCH INTENSITIES

Further increasing the rf power at −90 deg synchronous phase leads to an increasing energy spread of the bunch again (see Fig. 4). Due to the strict linear relation between energy and phase of the particles within the bunch, as they all started from a picosecond short bunch in the beginning, this allows for overrotating in phase space and therefore a temporal bunch compression along a drift behind the cavity. Our simulations predict an accessible bunch duration in the sub-ns domain, which gives access to peak particle currents of 10^{10} protons/ns with the current parameters of the beam line. This value has to be seen in the context of conventional available LINAC parameters. For comparison reasons, here the design values for the planned proton LINAC for FAIR [26] will be taken: 7×10^{12} protons in a 36 μs short bunch at 325 MHz, thus 6×10^8 protons/ns in one rf bucket, which is more than one order of magnitude less. Although laser-driven ion accelerators are still drastically lacking the average power (i.e., repetition rate), which is more important for most applications, they today govern a niche for special applications, that require (conventionally not accessible) highest particle intensities on shortest time scales in the mid-MeV energy region (necessary, e.g., in material science or for diagnosing transient short-time phenomena).

VII. SUMMARY AND OUTLOOK

A TNSA based compact (total length: 3 m) proton beam line has been successfully commissioned at GSI Darmstadt, using the PHELIX laser as driver of the proton acceleration. A pulsed high-field solenoid provides for beam capturing and energy selection and a rf cavity provides for energy compression, thus accessing the smallest energy spread (or in future experiments the shortest bunch duration via phase focusing) at high particle current. In the presented experiments from the latest campaign at this new beam line, intense proton bunches at 9.7 MeV energy and with particle numbers within the FWHM of the bunch of 1.7×10^9 ($\pm 15\%$) and an energy spread of $(2.7 \pm 1.7)\%$ have been measured.

Further optimization of this beam line is planned to increase the proton numbers, reach shortest possible bunch durations and implement additional (transverse) focusing elements to the beam line to access highest intensities.

ACKNOWLEDGMENTS

The authors want to specially thank the PHELIX laser team and the HF group at GSI for their work on the realization of this experimental campaign. This work is supported by HIC4FAIR.

[1] M. Roth, T. E. Cowan, M. H. Key, S. P. Hatchett, C. Brown, W. Fountain, J. Johnson, D. M. Pennington, R. A. Snavely, S. C. Wilks, K. Yasuike, H. Ruhl, F. Pegoraro, S. V. Bulanov, E. M. Campbell, M. D. Perry, and H. Powell, Phys. Rev. Lett. **86**, 436 (2001).

[2] P. K. Patel, A. J. Mackinnon, M. H. Key, T. E. Cowan, M. E. Foord, M. Allen, D. F. Price, H. Ruhl, P. T. Springer, and R. Stephens, Phys. Rev. Lett. **91**, 125004 (2003).

[3] G. M. Dyer, A. C. Bernstein, B. I. Cho, J. Osterholz, W. Grigsby, A. Dalton, R. Shepherd, Y. Ping, H. Chen, K. Widmann, and T. Ditmire, Phys. Rev. Lett. **101**, 015002 (2008).

[4] A. Pelka, G. Gregori, D. O. Gericke, J. Vorberger, S. H. Glenzer, M. M. Günther, K. Harres, R. Heathcote, A. L. Kritcher, N. L. Kugland, B. Li, M. Makita, J. Mithen, D. Neely, C. Niemann, A. Otten, D. Riley, G. Schaumann, M. Schollmeier, A. Tauschwitz, and M. Roth, Phys. Rev. Lett. **105**, 265701 (2010).

[5] S. Karsch, S. Düsterer, H. Schwoerer, F. Ewald, D. Habs, M. Hegelich, G. Pretzler, A. Pukhov, K. Witte, and R. Sauerbrey, Phys. Rev. Lett. **91**, 015001 (2003).

[6] A. J. Mackinnon *et al.*, Rev. Sci. Instrum. **75**, 3531 (2004).

[7] M. Roth *et al.*, Phys. Rev. Lett. **110**, 044802 (2013).

[8] K. Nemoto, A. Maksimchuk, S. Banerjee, K. Flippo, G. Mourou, D. Umstadter, and V. Y. Bychenkov, Appl. Phys. Lett. **78**, 595 (2001).

[9] I. Hofmann, J. M. ter Vehn, X. Yan, and H. Al-Omari, Nucl. Instrum. Methods Phys. Res., Sect. A **681**, 44 (2012).

[10] S. C. Wilks, A. B. Langdon, T. E. Cowan, M. Roth, M. Singh, S. Hatchett, M. H. Key, D. Pennington, A. MacKinnon, and R. A. Snavely, Phys. Plasmas **8**, 542 (2001).

[11] R. A. Snavely *et al.*, Phys. Rev. Lett. **85**, 2945 (2000).

[12] T. E. Cowan *et al.*, Phys. Rev. Lett. **92**, 204801 (2004).

[13] K. Harres, I. Alber, A. Tauschwitz, V. Bagnoud, H. Daido, M. Gunther, F. Nürnberg, A. Otten, M. Schollmeier, J. Schutrumpf, M. Tampo, and M. Roth, Phys. Plasmas **17**, 023107 (2010).

[14] T. Burris-Mog, K. Harres, F. Nürnberg, S. Busold, M. Bussmann, O. Deppert, G. Hoffmeister, M. Joost, M. Sobiella, A. Tauschwitz, B. Zielbauer, V. Bagnoud, T. Herrmannsdoerfer, M. Roth, and T. E. Cowan, Phys. Rev. ST Accel. Beams **14**, 121301 (2011).

[15] M. Schollmeier *et al.*, Phys. Rev. Lett. **101**, 055004 (2008).

[16] M. Nishiuchi *et al.*, Appl. Phys. Lett. **94**, 061107 (2009).

[17] M. Ikegami *et al.*, Phys. Rev. ST Accel. Beams **12**, 063501 (2009).

[18] J. Teng, Y. Gu, B. Zhu, W. Hong, Z. Zhao, W. Zhou, and L. Cao, Nucl. Instrum. Methods Phys. Res., Sect. A **729**, 399 (2013).

[19] S. Sinigardi, G. Turchetti, P. Londrillo, F. Rossi, D. Giove, C. De Martinis, and M. Sumini, Phys. Rev. ST Accel. Beams **16**, 031301 (2013).

[20] S. Busold *et al.*, Nucl. Instrum. Methods Phys. Res., Sect. A **740**, 94 (2014).

[21] V. Bagnoud *et al.*, Appl. Phys. B **100**, 137 (2010).

[22] S. Busold, D. Schumacher, O. Deppert, C. Brabetz, S. Frydrych, F. Kroll, M. Joost, H. Al-Omari, A. Blažević, B. Zielbauer, I. Hofmann, V. Bagnoud, T. E. Cowan, and M. Roth, Phys. Rev. ST Accel. Beams **16**, 101302 (2013).

[23] F. Nürnberg, M. Schollmeier, E. Brambrink, A. Blazevic, D. C. Carroll, K. Flippo, D. C. Gautier, M. Geissel, K. Harres, B. M. Hegelich, O. Lundh, K. Markey, P. McKenna, D. Neely, J. Schreiber, and M. Roth, Rev. Sci. Instrum. **80**, 033301 (2009).

[24] CST, http://www.cst.com/products/cstps.

[25] cea, http://irfu.cea.fr/sacm/logiciels/index3.php

[26] FAIR, https://www.gsi.de.